Lab on a Chip

Accepted Manuscript

ROYAL SOCIETY OF CHEMISTRY

www.rsc.org/loc

Table of content

We present an antibody-free approach for high throughput and purity dielectrophoretic isolation of CTCs from blood in a microfluidic chip.

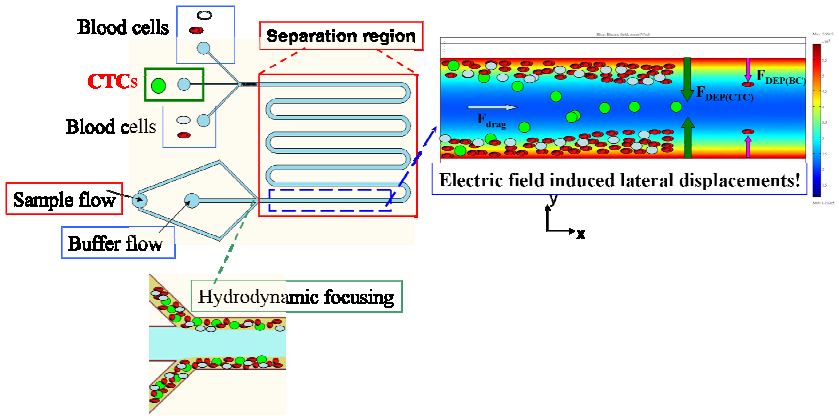

Antibody-Free Isolation of Rare Cancer Cells from Blood based on 3D Lateral Dielectrophoresis

I-Fang Cheng[1*], Wei-Lung Huang[2], Tzu-Ying Chen[1], Chien-Wei Liu[3], Yu-De Lin[1], Wu-Chou Su[2,4*]

[1]*National Nano Device Laboratories, National Applied Research Laboratories, Tainan, Taiwan*

[2]*Department of Internal Medicine, National Cheng Kung University College of Medicine and Hospital, Tainan, Taiwan*

[3]*Department of Mechanical Engineering, National Yunlin University of Science and Technology, Yunlin, Taiwan*

[4]*Cancer Center, National Cheng Kung University Hospital, Tainan, Taiwan*

*Corresponding Author:

I-Fang Cheng

E-mail: ifcheng@narlabs.org.tw

Wu-Chou Su:

E-mail: sunnysu@mail.ncku.edu.tw

Abstract

We present an antibody-free approach for the high-purity and high-throughput dielectrophoretic (DEP) isolation of circulating tumour cells (CTCs) from blood in a microfluidic chip. A hydrodynamic sheath flow is designed upstream in the chip to focus the suspension samples to the channel side walls, thus providing a queue to allow DEP-induced lateral displacements. High-throughput continuous cancer cell sorting (maximum flow rate: ~2.4 mL/h, linear velocity: ~4 mm/s) is achieved with a sustained 3D lateral DEP (LDEP) particle force normal to the continuous through-flow. This design allows the continuous fractionation of micro-/nanosized particles into different downstream subchannels based on the differences in their different critical negative DEP strengths/mobilities. The main advantage of this separation strategy is that increasing the channel length can effectively increase the throughput proportionally. The effective separation of rare cancer cells (<0.001%) from diluted human blood in a handheld chip is demonstrated. An enrichment factor of 10^5 and recovery rate of ~85% from a 0.001% cancer cell sample is achieved at an optimal flow rate of 20 μL/min passing through a 6-cm-long LDEP channel and an appropriate voltage at a frequency of 10 kHz. A higher throughput of 2.4 mL/h is also achieved with a 13-cm-long metal-based microchannel.

Key words: isolation, circulating tumour cells, dielectrophoresis

Introduction

Cancer cells that detach from a tumour, enter blood vessels, and circulate in the circulatory system are called circulating tumour cells (CTCs). CTCs can be used for the in-vitro diagnosis and assessment of cancers/tumours[1]. CTCs can provide a considerable amount of real-time information for cancer diagnoses such as localized cancer identification, drug susceptibility assessment, therapeutic monitoring, and prognosis assessment/tracking[2]. Furthermore, the number of CTCs can be used to evaluate the cancer prognosis and relapse, making it possible to predict cancer progression[3]. Therefore, there is a strong need for the early detection and assessment of CTCs, because this can enable early treatment. However, before analyses such as cell counting, prognosis and metastasis assessment, and identification of localized tumour cells can be conducted, it is very important to ensure the high recovery isolation of CTCs from blood.

The density gradient centrifugation method is used most commonly to isolate target cells from a heterogeneous medical sample[4]. However, this method fails in the case of low purity, recovery rate, and cell viability, as these conditions do not meet the requirements for further analysis and assessment. Alternatively, large, expensive equipment and the use of flow cytometry have been successfully used for isolating and counting CTCs using fluorescence- or magnetic-bead-based cell sorting systems[5,

[6]. However, such platforms limit the success rate of separating CTCs and further applications owing to the laborious sample preparations involved, which introduce artifacts or lead to the loss of the desired cells.

Antibody-based methods have proved popular for specifically capturing CTCs. In these methods, CTCs are captured using specific tumour antibodies such as epithelial-specific cell adhesion molecule (EpCAM) and cytokeratins (CKs)[7, 8]. Microfluidics and BioMEMS technologies have enabled low-cost, portable, and automatic operation as well as higher efficiency of antibody-specific binding for CTC isolation owing to their high surface-to-volume ratio[9, 10]. Biomarker-based isolation methods such as a modified antibody in a micropillar array[10-12] and nanoroughened surfaces in a microfluidic channel[13] have been developed to specifically capture CTCs in a microfluidic chip. Furthermore, immunomagnetic bead-based systems have been used for the isolation of CTCs and subsequent culture of rare CTCs in a microfluidic chip[14]. Unfortunately, some CTCs may show low or no EpCAM/CK expression on the cell membrane, and therefore, they cannot be effectively captured using the proposed biomarkers[15, 16]. Furthermore, the use of expensive antibodies results in additional costs related to detection and time consumption in conjugation/immobilization processes (typically 4–8 h).

In contrast, antibody-free approaches isolate CTCs without relying on antibodies

or biomarkers for specifically capturing tumour cells. Instead, they isolate cells based on different physical properties such as size, dielectric properties, and shapes intrinsic to cancer cells and blood cells[17, 18]. Microfluidic filters and membranes capture CTCs by size selection[19, 20]. Nevertheless, cell clogging limits their success, and high shear stress on the cell surface could significantly influence the cell viability during filtration[20]. Hydrodynamic mechanisms, such as inertial force and centrifuge force in a microchannel design, have been developed over the last few years to achieve size separation based on the size difference between CTCs and blood cells[21-23]. However, the purity of the isolated CTCs is relatively low (0.5%–10%) when the sample purity is lower than 0.1%[24].

Dielectrophoresis (DEP) provides more effective and flexible (real-time controllable) separation based on the size and dielectric properties[24-26]. Noncontact DEP approaches can also reduce cell damage, thus increasing the possibility of further analysis and assessment. Several strategies such as DEP gates[27-29], light-induced DEP (LIDEP)[30, 31], side-wall DEP[32], traveling-wave DEP (twDEP)[33, 34], and DEP-field flow fraction (DEP-FFF)[35] have been reported to precisely separate particles based on size using the DEP force as a function of particle volume r^3. In general, the DEP force can only affect local particles in short range because the decay relation of the electric field depends on the electrode shape and distance. For large distances relative to the

electrode size, the field strength decays with d^{-1} for a distant counter electrode. For a 2D planar electrode configuration, too, the electric field decays exponentially with the distance from the electrodes along the z-direction[25], thus causing particle separation to be characterized by a short range and low throughput (0.1–3 μL/min)[17, 36]. High-throughput and high-purity separation is required for CTC isolation because the number of CTCs is generally relatively low compared to the number of blood cells (1–10000 CTCs/mL in human blood, i.e., 10^{-3}% to 10^{-7}% of the total number of cells in blood). Therefore, short-range DEP separation designs cannot meet the requirements of practical applications.

In this study, we propose an antibody-free and long-range 3D DEP microfluidic platform for the effective and high-throughput isolation of rare cancer cells from diluted human blood. Our design uses a V-shaped microchannel with a long-range electric field gradient that induces a lateral DEP (LDEP) force normal to the continuous through-flow, as shown in Figure 1(a). This mechanism provides a long residence time for dielectrophoretically manipulating CTCs and blood cells to their specific equilibrium positions in the microchannel. Bioparticles with different sizes, dielectric properties, and shapes show different LDEP velocities and equipment positions, resulting in the sorting of CTCs and blood cells to different downstream subchannels with high throughputs. The throughput of the LDEP chip could be 1–2

orders higher than that of conventional gate/barrier-based DEP separators (0.1–3 μL/min)[28, 30, 32]. As a proof-of-concept, PC14PE6/AS2-GFP (AS2-GFP) lung cancer cells were spiked into human blood to demonstrate the capability to isolate CTCs. The equilibrium position of the DEP force and the frequency-dependent LDEP migration rate for tumour cells and blood cells were investigated to optimize the separation conditions. The effective separation of rare cancer cells from diluted human blood in the chips is successfully demonstrated. To the best of our knowledge, no study has previously reported the use of a 3D long-range LDEP force normal to the continuous through-flow to achieve the high-throughput and high-purity isolation of CTCs.

Materials and Methods

Theory and chip design

DEP is the induced motion of a polarized dielectric particle by a nonuniform AC electric-field-induced polarization. The time-averaged DEP force is defined as

$$F_{DEP} = 2\pi r^3 \varepsilon_{\mathrm{m}} \,\mathrm{Re}[\, f_{CM}(\omega)]\, \nabla \mathrm{E}^2 \qquad (1)$$

where ε_{m} is the permittivity of the medium; r, the radius of the particle; and $\nabla \mathrm{E}^2$, the magnitude of the electric field gradient. The effective polarizability-Clausius-Mossotti (CM) factor f_{CM} is given by

$$f_{CM} = \frac{\varepsilon_p^* - \varepsilon_m^*}{\varepsilon_p^* + 2\varepsilon_m^*} \qquad (2)$$

ε_p^* and ε_m^* indicate the complex permittivity of the particle and the surrounding medium, respectively. The effect of the complex permittivity can be controlled by changing the frequency (ω) of the applied electric field and can be given as $\varepsilon^* = \varepsilon - i(\sigma/\omega)$. If particles are more or less polarizable than the surrounding medium, they will be moved to a region with relatively strong (positive DEP) or relatively weak (negative DEP) electrical field gradient, respectively. When an AC electric field is imposed on a cell suspended in a medium having much lower conductivity than the cell cytoplasm, f_{CM} may be approximated as[37, 38]

$$f_{CM} = \frac{f_1^2 - f_{co}^2}{f_1^2 + 2f_{co}^2} \quad (3)$$

f_1 represents the applied AC electric frequency and f_{co}, the crossover frequency (no particle DEP movements, $\mathrm{Re}[f_{CM}] = 0$). At sufficiently high frequency ($f > \sigma_m/C_{mem}$), the electric field can penetrate the cell membrane and the cytoplasm. The internal cytoplasmic conductivity of the cell, which is related to the external medium's conductivity, significantly influences the crossover frequency of a cell. f_{co} can be given as

$$f_{co} = \frac{1}{2\pi r C_{mem}} \sqrt{\frac{2\sigma_p\sigma_m - r g_{mem}(\sigma_p - 4\sigma_m)}{(\sigma_p + 2\sigma_m)(\sigma_m^{-1} - \sigma_p^{-1})} - g_{mem}^2 r^2} \quad (4)$$

where C_{mem} is the capacitance per unit area of the plasma membrane; σ_m, the conductivity of the external medium; σ_p, the internal cytoplasmic conductivity of the

particle; and g_{mem}, the specific membrane conductance. f_{co} is linearly dependent on the medium conductivity when the membrane conductivity is low and the cell cytoplasmic conductivity is much higher than the medium conductivity[39]. At frequencies higher than σ_m/C_{mem} and below 1 MHz, the crossover frequency of a spherical cell under these conditions can be approximated as[37, 38]

$$f_{co} \approx \frac{\sigma_m}{\sqrt{2}\pi r C_{mem}} \quad (5)$$

For a biological cell, the conductivity of the cell cytoplasm and cell membrane is much higher and much lower than that of the suspending medium, respectively. The cell will exhibit negative and positive DEP at relatively low and high frequencies, respectively[29, 38].

To produce a long-range electric field gradient with a long residence time inside the fluidic channel in order to continuously separate blood cells and cancer cells, we designed and fabricated inclined channel walls forming a V-shaped microchannel. An electric field was generated across the entire microfluidic channel between the top and the bottom conductive surfaces, and thus, a lateral electric field gradient was generated by the different distances between the top and the bottom potential sources (Figure 2(a). When an AC voltage was applied to the top planar and bottom V-shaped conductive surfaces of the entire microchannel, it produced varied electric field

strengths along the y-direction in the triangular fluid chamber, thus generating a long-range electric field gradient. Therefore, LDEP forces were induced on the particle to produce lateral displacements normal to the continuous through-flow. Unlike the isolated electrodes, the gradient of the electric field and the DEP force are both sustained for the entire long channel. By doing so, target cells can be isolated in one part of the channel, either to the middle or to the sides, depending on the particle size and applied frequency. Balancing the DEP force with viscous drag for a particle of size r in a medium with viscosity η provides a linear LDEP particle velocity normal to the through-flow given as

$$V_{DEP}(y) = \frac{r^2 \varepsilon_{\mathrm{m}} \mathrm{Re}[f_{CM}(\omega)] \nabla \mathrm{E}^2(y)}{3\eta} \quad (6)$$

The DEP force strongly depends on the volume of the particle ($F_{DEP} \sim r^3$) and the gradient of the applied electric field. Therefore, the DEP mechanism can be used for precise size separation. Based on equation (3), the LDEP velocity also depends on the applied voltage, frequency, and particle size and the dielectric properties. The equilibrium position of a cell is at the position where the induced particle DEP force balances the viscous drag force in the y-direction. Therefore, the final equilibrium position of each cell population depends on the cell DEP strength that is induced by the electric field gradient in the y-direction.

Experimental setup and microfabrication

An AC voltage was supplied by a multi-output waveform generator (Wavetek, model 195) that was applied to the DEP-based microfluidic chip to induce the LDEP forces. Two portable peristaltic fluid pumps (LongerPump®, BT100-2J) were used to continuously inject the sample and buffer flows in 1:3 ratio through a 10-mL fluid chamber. The experiment was observed through an inverted fluorescence microscope (IX71, Olympus), and the experimental results were recorded in both video and photo formats using a CCD camera (30 frames/s, *Microfire,* OPTRONICS). The particle velocities and their final positions were analysed using Image-Pro Plus 6.0 software (MediaCybernetics).

A 1-μm-thick silicon nitride (Si_3N_4) layer was deposited on a Si-wafer with a crystallographic plane of 110. A positive photoresist, AZ 5214, was patterned on Si_3N_4 by a standard photolithography technique, and then, the exposed Si_3N_4 was etched using inductively coupled plasma dry etching. The patterned Si_3N_4 layer on the Si-wafer served as a passive mask during the KOH etching of the silicon. After the anisotropic wet-etching of the silicon wafer, sidewalls with 35° inclination were formed in the microchannel to form a V-shaped microchannel with 110° angle, 200-μm depth, and 700-μm width. Titanium (Ti, 40 nm) was deposited on the formed microchannel as an adhesion layer, and gold (Au, 200 nm) was subsequently

deposited on the Ti layer to serve as a conductive layer by an electron beam evaporator. Figure 1(b) shows an SEM image of the V-shaped conductive microchannel. The metallic microgroove was bonded with an ITO-coated glass slide using 10−μm-thick 3M double-sided tape to from the 3D LDEP device. The chip does not need to be patterned with the electrode geometry. Figure 1(c) shows the cross section of the microfluidic chip assembly. The chip has a face-to-face electrode configuration, a planar ITO electrode at the top, and a V-shaped groove with an Au-covered surface at the bottom of the channel to form a triangular fluid chamber. When an AC voltage was applied to the top planar and bottom V-shaped conductive surfaces, varied electric field strengths were generated along the y-direction to produce an electric field gradient along the entire channel (Figure 2(a). The fabrication processes for the 3D LDEP chips are relatively simple and do not require expensive equipment and time-consuming procedures as is the case with the electroplating-based 3D DEP chips and face-to-face DEP gates[27, 32]. The 3D metallic microchannel used to drive the DEP forces can be fabricated in three simple steps—microchannel fabrication, metal deposition, and chip bonding—thus eliminating the need for electrode patterning and precise alignment steps in the top and bottom layers.

Sample preparation

To easily distinguish the tumour cells from the blood cells by fluorescent microscopy, a GFP-expressing human lung adenocarcinoma cell line, PC14PE6/AS2-GFP (AS2-GFP), was used to study the separation capability and isolation efficiency of the proposed chip. We had previously established this cell line by stably transfecting the parental AS2 cells with GFP-expressing plasmid[40]. The AS2-GFP cells were maintained in MEM-α (Invitrogen, Carlsbad, CA, USA) with 10% foetal calf serum (FCS; Invitrogen) and incubated at 37°C in a humidified atmosphere containing 5% CO_2.

To investigate the isolation capability, the AS2-GFP cells were seeded 48 h before the experiments. The cells were grown to subconfluent densities and collected using trypsin. The trypsin was then neutralized using an FCS-supplemented medium. The cells were washed once and resuspended with the FCS-supplemented medium.

Leukocytes (WBCs) and erythrocyte (RBCs) were isolated from whole blood using Ficoll-Paque (GE Healthcare Life Sciences) density gradient separation for individually investigating the DEP properties of WBCs and RBCs. 3 mL of blood from a healthy human was carefully added to 3 mL of Ficoll buffer, and then, the sample was centrifuged at 2100 rpm for 20 min at 20–25°C. After centrifugation, the buffy coat of the PBMC and RBC were carefully taken out and individually

resuspended in the PBS buffer. Then, the cells were washed two times using the experimental buffer. Finally, the WBCs and RBCs were individually resuspended in 3 mL of the experimental buffer to further investigate the DEP behaviours. The final WBC and RBC concentrations were adjusted to ~5×10^5 cells/mL and 5×10^6 cells/mL, respectively.

An isotonic phosphate buffered saline (PBS) buffer diluted with 280 mM sucrose in 1:20 ratio (σ_m ~0.78 mS/cm) was used as the experimental buffer because human cells are highly sensitive to the osmotic pressure of a solution. Human blood cells were diluted 20 times (~2.3×10^8 cells/mL) using the experimental buffer to avoid blood cell coagulation. The diluted blood samples were spiked with cancer cell concentrations of 6×10^2, 3×10^3, and 3×10^4 cells/mL to investigate the separation capability in the 3D LDEP platform.

Evaluation of purity and recovery rate of tumour cell isolation

We used two different methods to determine the cell concentrations and tumour/blood ratios in the samples and sorted products. First, the samples were evaluated using a Countess automated cell counter (Invitrogen) according to the manufacturer's instructions. Briefly, 6 μL of the cell-containing sample was taken and mixed with trypan blue in 1:1 ratio. Then, 10 μL of the mixture was loaded into a

counting slide chamber, and the cells were counted in the automated cell counter. A single sample measurement using this counter provided the following data: total cell concentration, cell viability, viable cells : total cells ratio, and cell size. After automated cell counting, we further subjected the counting slide to fluorescent microscopy analysis. The cells were counted in five random fields at 100x magnification under a Nikon Eclipse Ti fluorescent microscope with both bright light and green fluorescent images. We also subjected the samples to further fluorescence microscopy analysis.

Results and Discussions

Chip design and finite element simulation

Finite element simulations were conducted to predict the electric field distribution and its magnitude. They were solved numerically using finite element analysis software (Comsol Multiphysics 3.5, Comsol Ltd.). The electric scalar potential V satisfies Poisson's equation. The electric field and displacement were obtained from the gradient of V.

The short-range and local distribution of the electric field gradient is a key limitation for DEP-based manipulation techniques. Even when the field gradient was increased greatly through micro-/nanofabrication, the long-range manipulation of

particles was difficult to achieve in DEP separation systems. Our proposed 3D V-shaped electrode configuration provides a long-range field gradient in the entire channel. Figure 2(a) shows the electric field distribution for the proposed design. The field maxima locate at the channel side walls, and the field minima locate in the middle of the channel; this is because the electrode separation distance between the top and the bottom layers gradually decreases from the sidewalls of the channel to the middle region (Figure 2(b)). Therefore, the directions of the negative DEP force are toward the centre region of the channel, as shown in Figure 2(b). In Figure 2(b), the arrows represent the directions of the normalized negative electric field gradient (direction of negative DEP force). In addition, the V-shaped and trapezoid metallic channels were used to compare the geometrical effect of the electric field distribution. The design of the trapezoid channel shows that the electric field distribution has two second minima field regions near the lower line, as shown in the supplementary material. On the other hand, the V-shaped design only has one minima field region in the middle of the channel (Figure 2(b)). Therefore, a triangular configuration may be more suitable for the negative DEP-based separation strategy. Compared to a 2D planar electrode-based DEP, the 3D electric field gradient design also minimizes decays in the DEP force, such that both forces increase monotonically with voltage to further increase the throughput.

Lateral Migration Velocities and Equilibrium Positions

The DEP velocity spectra of RBC, WBC, and AS2-GFP cells were investigated to determine the appropriate frequencies for effectively separating cancer cells and blood cells in a continuous through-flow. The velocity was calculated by measuring the time taken for individual cells to move a given distance from the channel side wall toward an equilibrium position (negative LDEP) or a distance from a position toward the channel side wall (positive LDEP), with a time interval of 0.1 s/frame. Figure 3(a) shows the measured results of cell velocity versus applied frequency when a constant voltage of 20 V_{pp} was applied. The velocity profiles indicate that the cells induced a negative and a positive DEP force at relatively low and relatively high frequencies, respectively. The cross-over frequency of RBC, WBC, and AS2-GFP cells was measured at 600–700, 300–400 and 100–200 kHz, respectively. High differences occurred in the LDEP velocity between the AS2-GFP cells and the blood cells at frequencies lower than 50 kHz and higher than 400 kHz. To avoid cell adhesion to the channel surface at high frequencies (positive DEP) and bobble generation at low frequencies (lower than 2 kHz), a frequency of 10 kHz was chosen for future investigations and cell separation.

The DEP velocity increases/decreases with a square relationship of the electric

field gradient and particle size. Therefore, the large difference in the particle size of cancer cells and blood cells could induce different lateral migration velocities and cause stopping at different equilibrium positions under a predetermined electrical condition. Therefore, the appropriate frequencies for the separation of AS2-GFP cells, WBCs, and RBCs were first investigated, and a frequency of 10 kHz was set to measure the equilibrium positions of these three types of cells. Cell equilibrium occurs at the position where the particle DEP force balances the fluid viscous force in the microchannel. In our design, the electric field strength gradually reduces from the channel side walls toward the centre of the microchannel. The results show that the equilibrium positions are very different in the cancer cells and blood cells owing to the different cell sizes, causing a difference in their corresponding threshold DEP forces at different positions in the y-direction (AS2-GFP: 15–25 μm, WBC: 8–12 μm, RBC: 6–8 μm[38]). The result also showed that the induced LDEP velocity increased with the applied AC voltage (Figure 3(b)), and the equilibrium positions presented toward the middle of the channel when the applied voltage increased, as shown in Figure 3(c). The results show that the equilibrium positions of WBCs and RBCs are very close, and their experimental images are very similar. Therefore, we only showed the equilibrium position images of blood cells and AS2-GFP cells to highlight their differences (Figure 3(c1) and (c2)). Considering the equilibrium positions and

equilibrium time (Figure 3(b) and (c)), an optimal separation situation is given as

$$t_{DEP\_BC(y)} > t_{flow(x)} > t_{DEP\_CTC(y)} \quad (7)$$

Here, t_{flow} is the characteristic time required for the sample flow to pass through the length of the flowing channel l, $t_{flow} = l / v_{flow}(x)$, and t_{DEP} is the characteristic time as defined by the required time to transport a specific cell from an initial position to the equilibrium position by a distance d, $t_{DEP} = d / v_{DEP}(y)$. $v_{flow}(x)$ and $v_{DEP}(y)$ are the sample flow velocity along the x-direction and the induced cell DEP velocity along the y-direction, respectively. The separation distance between the two types of cells can be defined as $d_{separation} = \left|(d_{eq1} - v_{DEP1} \times t_{flow}) - (d_{eq2} - v_{DEP2} \times t_{flow})\right|$, where d_{eq1} and d_{eq2} is the equilibrium position for cell 1 and cell 2, respectively. Therefore, the optimal separation situation depends on the particle residence time in the DEP field versus the flow transition time and the differences in the equilibrium positions between the CTC and the blood cells.

Continuous sorting of cancer cells from blood

The sample and buffer flow rates were applied in 1:3 ratio, and thus, the sample flow with the suspended cancer cells and blood cells can both be collected as two particle streams along the side walls of the channel. Under this condition, the flowing sample stream involving blood cells and AS2-GFP cells can be collected at a distance

of 150–200 μm from the channel side walls (Figure 4(a)). The AS2-GFP cells and blood cells both flowed into the upper and lower subchannels when no electric field was applied (Figure 4(b)). In this DEP microfluidic chip, the fluorescent AS2-GFP cells and blood cells flowed along the x-direction of a 6-cm-long channel, and an external AC electric field (an applied voltage of 18 V_{pp} at a frequency of 10 kHz) was applied to produce DEP forces perpendicular to the flow direction (along the y-direction). When the flowing cells entered the LDEP field regions, a negative LDEP force pushed them toward the centre of the channel. Here, the AS2-GFP cells experienced a higher LDEP force that induced a longer lateral displacement to be manipulated into the middle region of the channel, as shown in Figure 4(c). On the other hand, the blood cells experienced a lower LDEP force that induced shorter displacements, and they could only be moved a distance of ~200 μm from the channel side walls (Figure 4(c)). These effects resulted in the separation of the CTCs and blood cells into the middle and upper/lower subchannels, respectively, as shown in Figure 4(d). The figure shows very dense blood cells (~2.3×10^8 cells/mL) in the input sample wherein the AS2-GFP cells (~1200 CTCs/mL) are difficult to count and further analyse precisely (Figure 5(a) and (b)) because dense blood cells could hide the AS2-GFP cells and significantly interfere with the downstream molecular analysis. After the LDEP isolation, the sorted sample showed that the blood cells were greatly

reduced (roughly 4–5 orders of blood cells removed), as shown in Figure 5(b) and (c), and the number of CTCs could be counted and further analysed easily. Crystal violet staining showed that the viability of the isolated cancer cells reached ~85% (data not shown).

In a high-ionic-strength fluid, the electrothermal effect near the microelectrodes was also taken into consideration. The increase in the local temperature induced by the applied AC electric field can be calculated by $\Delta T \sim \sigma V_{rms}^2/k$ [41]. For the applied voltage of 18 V_{pp}, frequency of 5 kHz to 1 MHz, medium conductivity of 0.78 mS/cm, and thermal conductivity of k (1.0 W/mK), the temperature rise can be estimated to be only ~6.2°C. In addition, a continuous through-flow separation system can reduce the Joule thermal effect near the electrode surface[42] owing to through-flow convection, especially when the flow passes through a high-thermal-conductivity material such as silicon[38]. Therefore, the separation process in the continuous flow chamber would not be influenced significantly. Furthermore, a negative DEP force from the top and bottom electrodes can also minimize sedimentation and field-induced lysis of the cells [43].

Recovery rate and isolation purity

The recovery rate is defined as the percentage of the isolated cancer cell number

over the initial spiked cancer cell number in the prepared blood sample. The predetermined optimal condition (18 V_{pp} at 10 kHz) was applied to a 6-cm-long LDEP channel wherein different flow rates were used to investigate the isolation performance. Figure 6(a) shows that the recovery rate can reach as high as 84%–92% and 81%–88% at a flow rate of 10 and 20 μL/min, respectively. Furthermore, as the flow rate increases to 30 μm/min, the recovery rate decreases significantly to ~60%. This result could be attributed to the fact that the cell transportation time in the through-flow is shorter than the characteristic LDEP time when the flow rate is higher than 20 μL/min. The experimental results also indicate that the cell concentration does not significantly influence the isolation recovery. The experimental results show that an isolation purity of 81.6%, 91.3%, and 87% was achieved at a flow rate of 10, 20, and 30 μL/min, respectively, when the original cancer cell purity was 0.01% (Figure 6(b)). Therefore, the results show an excellent enrichment factor of ~10^5 in our LDEP sorter. In our observation, a higher flow rate leads to a higher capability for blood cell depletion. However, the recovery also decreased significantly when the flow rate was as high as 30 μL/min. The coupled effects resulted in lower isolation purity compared to that under the optimal flow rate of 20 μL/min (Figure 6(b)). Considering the high isolation purity, recovery, and throughput, the recommended flow rate for LDEP CTC isolation was set at 20 μL/min to achieve high enrichment of 10^5 and high recovery

rate greater than 85%.

Ideally, the proposed separation strategy involves increasing the channel length to effectively increase the throughput. Therefore, to prove this concept, a 13-cm-long serpentine DEP channel was used to isolate cancer cells from the diluted blood at a higher flow rate of 40 μL/min. Figure 6(c) shows the isolation recovery at flow rates of 20 and 40 μL/min using a 6- and 13-cm-long LDEP channel, respectively. The cells in a 6-cm-long LDEP microchannel experienced a shorter particle residence time in the DEP field, and the experimental results show that the recovery decreased significantly when the flow rate was increased to 40 μL/min. On the other hand, the cells in a 13-cm-long DEP microchannel experienced a longer LDEP affecting time, and thus, the recovery reached ~81% and only decreased slightly (<10%) when the flow rate increased up to 40 μL/min. The results confirm that the proposed isolation strategy can increase the isolation throughput by increasing the particle residence time in the LDEP field, which is in good agreement with the numerical predictions.

Conclusions

We have extensively characterized the proposed LDEP-based microfluidic chip by varying the applied AC voltage, frequency, sample flow rate, and length effect of the LDEP channel and optimizing these parameters for the isolation purity, recovery,

and throughput. Compared to conventional physical methods (purity = ~0.5%–10%), immunomagnetics-based methods, and microfluidic biomarker-based methods, the isolation purity, recovery rate, throughput, and viability of the proposed antibody-free chip were excellent, especially with regard to high enrichment at high flow rate (>20 μL/min). The recovery was greater than 85%, and the isolation purity was greater than 90% when the original cancer cell purity was 0.01% (enrichment factor: ~10^5). The great advantage of this separation strategy is that increasing the channel length to prolong the particle residence time in the LDEP field can effectively increase the throughput proportionally. For proof of the proposed concept, 2.4 mL/h isolation throughput with a recovery rate as high as 81% was achieved within a 13-cm-long LDEP-based microchannel. Under this condition, a 5 mL sample volume could be isolated in ~2 h, and blood cells could be removed with a depletion rate of 10^5. On-chip analysis of the isolated cells is ongoing and expected to be applicable for many detection approaches such as electrical and optical spectra analysis approaches.

Acknowledgements

This work was supported by the Ministry of Science and Technology of Taiwan (MOST 102-2221-E-492-001-MY2, MOHW 103-TD-B-111-06 and MOHW103-TDU-B-211-113002). We also thank the National Nano Device Laboratory for supplying the micro-fabrication equipment.

References

1. V. Zieglschmid, C. Nollmann and O. Bocher, Crit. Rev. Clin. Lab., 2005, **42**, 155.

2. L. Yu, S. R. Ng, Y. Xu, H. Dong, Y. J. Wang and C. M. Li, Lab Chip, 2013, **13**, 3163.

3. S. Mocellin, D. Hoon, A. Ambrosi, D. Nitti and C. R. Rossi, Clin. Cancer Res., 2006, **12**, 4605.

4. Z. S. Lalmahomed, J. Kraan, J. W. Gratama, B. Mostert, S. Sleijfer and C. Verhoef, J. Clin. Oncol., 2010, **28**, 288.

5. S. M. B. Fong, M. K. Lee, P. S. Adusumilli and K. J. Kelly,Surgery, 2009, **146**, 498.

6. P. K. Y. Goon, C. J. Boos, P. S. Stonelake, A. D. Blann, G. Y. H. Lip, *Thromb. Haemost.*, 2006, **96**, 45-52.

7. G. Deng, M. Herrler, D. Burgess, E. Manna, D. Krag and J. F. Burke, *Breast Cancer Res.*, 2008, **10**, 69.

8. F. I. Thege, T. B. Lannin, T. N. Saha, S. T., M. L. Kochman, M. A. Hollingsworth, A. D. Rhim and B. J. Kirby, *Lab Chip***,** 2014,**14**, 1775.

9. S. Wang, H. Wang, J. Jiao, K.-J. Chen, G. E. Owens, K. Kamei, J. Sun, D. J. Sherman, C. P. Behrenbruch, H. Wu and H.-R. Tseng, Angew. Chem. Int. Ed., 2009, **48**, 8970.

10. S. Nagrath, L. V. Sequist, S. Maheswaran, D. W. Bell, D. Irimia, L. Ulkus, M. R. Smith, E. L. Kwak, S. Digumarthy, A. Muzikansky, P. Ryan, U. J. Balis, R. G. Tompkins, D. A. Haber and M. Toner, *Nature*, 2007, **450**, 1235.

11. J. Xia, X. Chen, C. Z. Zhou, Y. G. Li and Z. H. Peng, *IET Nanobiotechnol.*, 2011, 5, 114–120.

12. T. Ohnaga, Y. Shimada, M. Moriyama, H. Kishi, T. Obata, K. Takata, T. Okumura, T. Nagata, A. Muraguchi and K. Tsukada, Biomed. Microdevices, 2013, **15**, 611.

13. W. Chen, S. Weng, F. Zhang, S. Allen, X. Li, L. Bao, R. H. W. Lam, J. A. Macoska, S. D. Merajver and J. Fu, *ACS nano*, 2013, **7**, 566.

14. J. H. Kang, S. Krause, H. Tobin, A. Mammoto, M. Kanapathipillai and D. E. Ingber, *Lab Chip*, 2012, **12**, 2175.

15. S. D. Mikolajczyk, L. S. Millar, P. Tsinberg, S. M. Coutts, M. Zomorrodi, T.

Pham, F. Z. Bischoff and T. J. Pircher, *Oncology*, 2011, **10**, 252361.

16. P.T.H. Went, A. Lugli, S. Meier, M. Bundi, M. Mirlacher, G. Sauter and S. Dirnhofer, Hum. Pathol., 2004, **35**, 122.

17. I. Cima, C. W. Yee, F. S. Iliescu, W. M. Phyo, K. H. Lim, C. Iliescu and M. H. Tan, *Biomicrofluidics*, 2013, **7**, 011810.

18. A. Karimi, S. Yazdi and A. M. Ardekani, Biomicrofluidics, 2013, **7**, 021501.

19. H. Mohamed, L. D. McCurdy, D. H. Szarowski, S. Duva, J. N. Turner and M. Caggana, IEEE Trans. Nanobiosci., 2004, **3**, 251.

20. S. J. Tan, R. L. Lakshmi, P. F. Chen, W. T. Lim, L. Yobas and C. T. Lim, Biosens. Bioelectron., 2010, **26**, 1701.

21. A. A. S. Bhagat, H. W. Hou, L. D. Li, C. T. Lim and J. Y. Han, *Lab Chip*, 2011, **11**, 1870.

22. H. W. Hou, M. E. Warkiani, B. L. Khoo, Z. R. Li, R. A. Soo, D. S.-W. Tan, W.-T. Lim, J. Han, A. A. S. Bhagat and C. T. Lim, *Sci. Rep.*, 2013, **3**, 1259.

23. A. J. Mach, J. H. Kim, A. Arshi, S. C. Hurab and D. D. Carlo, *Lab Chip*, 2011, **11**, 2827.

24. H.-S. Moon, K. Kwon, S.-I. Kim, H. Han, J. Sohn, S. Lee and H.-I. Jung, *Lab Chip*, 2011, **11**, 1118.

25. I-F. Cheng, H.-C. Chang, T.-Y. Chen, C. Hu and F.-L. Yang, *Sci. Rep.*, 2013, **3**, 2365.

26. K.-H. Han, S.-I Hana and A. B. Frazier, *Lab Chip*, 2009, **9** 2958.

27. T. Müller, A. Pfennig, P. Klein, G. Gradl, M. Jäger, and T. Schnelle, IEEE Eng. Med. Biol. Mag., 2003, **22**, 51.

28. M. Alshareef, N. Metrakos, E. J. Perez, F. Azer, F. Yang, X. Yang and G. Wang, Biomicrofluidics, 2013, **7**, 011803.

29. I-F. Cheng, C.-C. Lin, D.-Y. Lin and H.-C. Chang, *Biomicrofluidics*, 2010, **4**, 034104.

30. S.-B. Huang, M.-H. Wu, Y.-H. Lin, C.-H. Hsieh, C.-L. Yang, H.-C. Lin, C.-P. Tseng and G.-B. Lee, *Lab Chip*, 2013, **13**, 1371.

31. I-F. Cheng, S.-L. Liu, C.-C. Chung and H.-C. Chang, *Microfluid Nanofluid*, 2012,

12, 95.

32. G. Mernier, E. Duqi and P. Renaud, *Lab Chip*, 2012, **12**, 4344.

33. I-F. Cheng, V. Froude, Y.-E. Zhu, H.-C. Chang and H.-C. Chang, *Lab Chip*, 2009, **9**, 3193.

34. Y. Huang, X. B. Wang, J. A. Tame and R. Pethig, J. Phys. D: Appl. Phys., 1993, **26**, 1528.

35. V. Gupta, I. Jafferji, M. Garza, V. O. Melnikova, D. K. Hasegawa, R. Pethig and D. W. Davis, *Biomicrofluidics*, 2012, **6**, 024133.

36. S. Bose, R. Singh, M. Hanewich-Hollatz, C. Shen, C.-H. Lee, D. M. Dorfman, J. M. Karp and R. Karnik, *Sci. Rep.*, 2013, **3**, 2329.

37. J. Gimsa, P. Marszalek, U. Loewe, and T. Y. Tsong, Biophys. J., 1991, **60**, 749.

38. P. R. C. Gascoyne, S. Shim, J. Noshari, F. F. Becker and K. Stemke-Hale, Electrophoresis, 2013, **34**, 1042.

39. J. Gimsa, M. Stubbe, and U. Gimsa, J. Electr. Bioimp., 2014, 5, 74.

40. H. H. Yeh, W. W. Lai, H. H. Chen, H. S. Liu, W. C. Su, Oncogene, 2006 , **25**, 4300.

41. C. Rosales, Electrophoresis, 2006, **27**, 1984.

42. C. Iliescu, G. L. Xu, V. Samper and F. E. H. Tay, J. Micromech. Microeng., 2005, **15**, 494.

43. P. R. C. Gascoyne, J. Noshari, T. J. Anderson and F. F. Becker, Electrophoresis, 2009, **30**, 1388.

Figure captions

Figure 1 The LDEP CTC isolation system. (a) The induced LDEP forces on the blood cells and CTC produce different LDEP velocities normal to the through-flow and balance the fluid viscosity at different equilibrium positions, resulting in the sorting of CTCs and blood cells to different downstream subchannels. (b) SEM image of a V-shaped conductive microchannel. (c) Cross-sectional diagram of the microfluidic chip assembly.

Figure 2 Finite element simulation of electric field for 3D V-shaped and trapezoid electrode configurations. (a) The electric field was generated across the entire microfluidic channel between the top and the bottom conductive surfaces, and therefore, it provides a long-range field gradient in the entire channel. (b) The lateral electric field gradient was generated by the different distances between the top and the bottom potential sources, and the V-shaped design only has one minima field region in the middle of channel.

Figure 3 (a) Experimentally determined LDEP velocity–frequency profile showing the appropriate range of applied frequencies for blood cell and CTC separation (data are averaged over three runs). (b) LDEP moving velocity of AS2-GFP, WBCs, and RBCs versus various applied voltages. (c) Various applied voltages versus the related equilibrium positions for RBCs, WBCs, and AS2-GFP cells, respectively.

Figure 4 (a) The flowing sample stream involving blood cells and AS2-GFP cells was collected at a distance of 150–200 μm from the channel side walls using hydrodynamic focusing. (b) Both cancer cells and blood cells flowed into the upper and lower subchannels when no electric field was applied. (c) When a determined electric field was applied, AS2-GFP cells experienced a higher LDEP force that induced a longer lateral displacement to be manipulated into the middle region of the channel. Blood cells experienced a lower LDEP force that induced a shorter displacement, and they were only transported to a distance of ~200 μm from the channel side walls. (d) Separation of cancer cells and blood cells into the middle and upper/lower subchannels, respectively.

Figure 5 (a) Very dense blood cells and rare AS2-GFP cells in the input sample, wherein the AS2-GFP cells are difficult to examine. (b) AS2-GFP cells in a very dense blood sample in a fluorescence field. (c) After DEP isolation, the sorted sample showed that the blood cells were greatly reduced. (d) Sorted AS2-GFP cells in the fluorescence field after DEP enrichment.

Figure 6 (a) The recovery rate at different flow rates achieved by using a LDEP chip. (b) The isolation purity versus different spiked AS2-GFP concentrations at different flow rates. (c) The isolation recovery at flow rates of 20 and 40 μL/min using a 6- and a 13-cm-long LDEP channel, respectively. The AS2-GFP cells in a 13-cm-long channel experienced a longer LDEP affecting time, and the recovery still reached ~80% when the flow rate increased up to 40 μL/min.

Figure 1

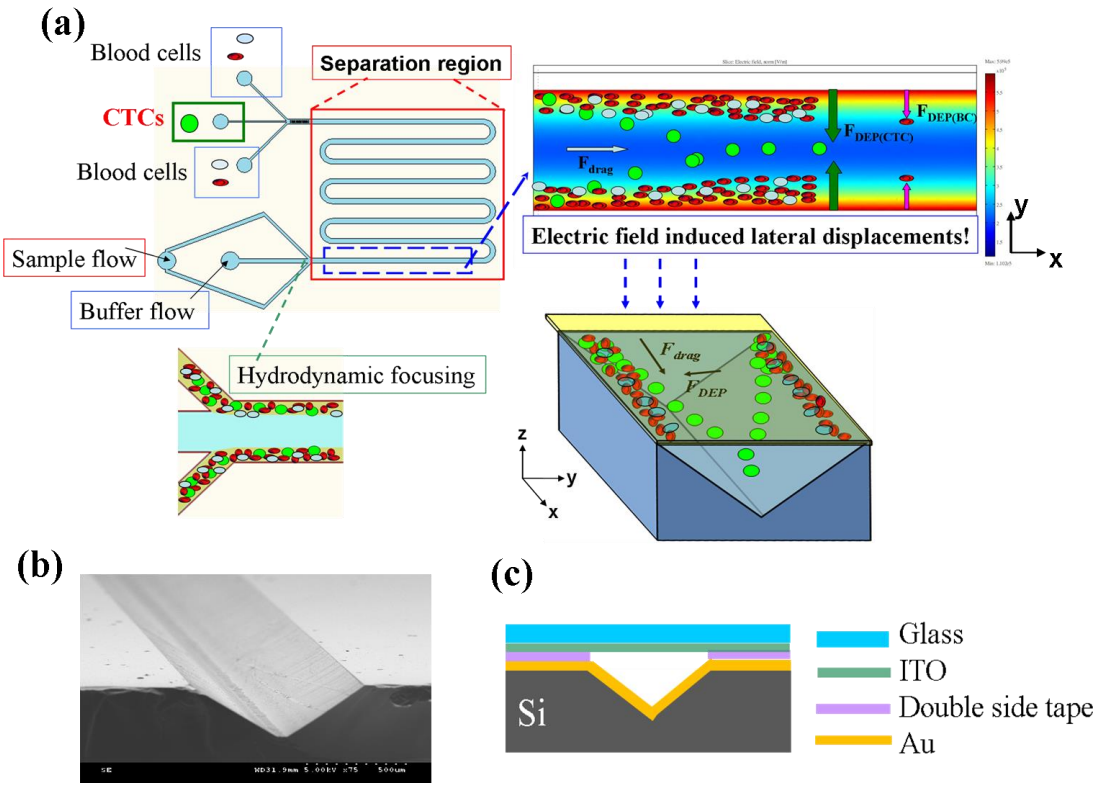

Figure 2

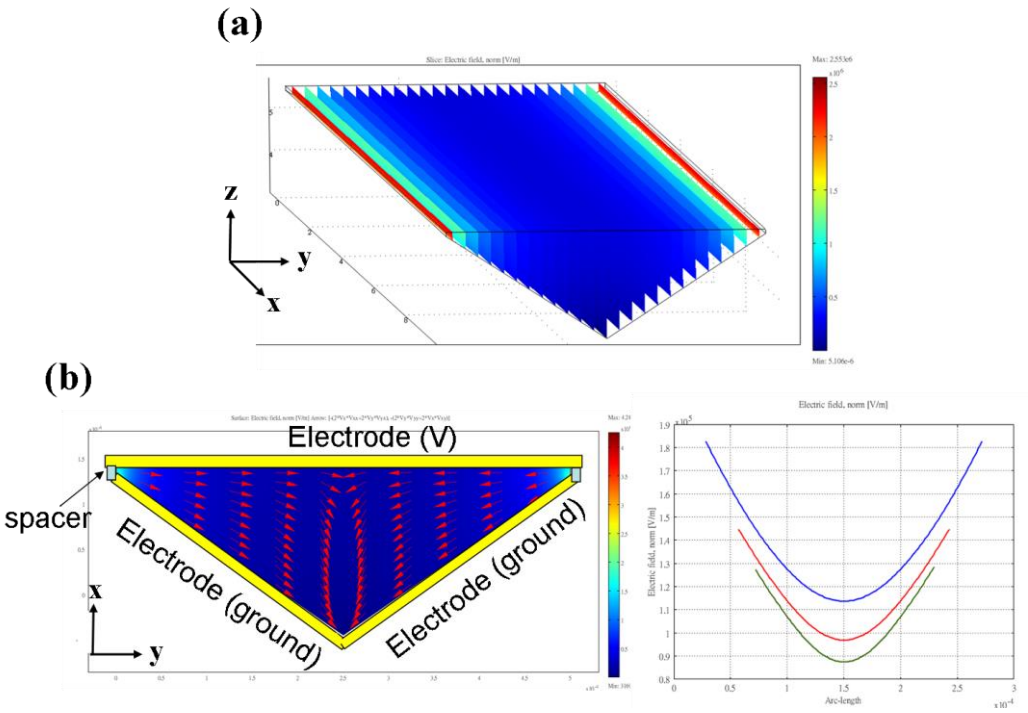

Figure 3

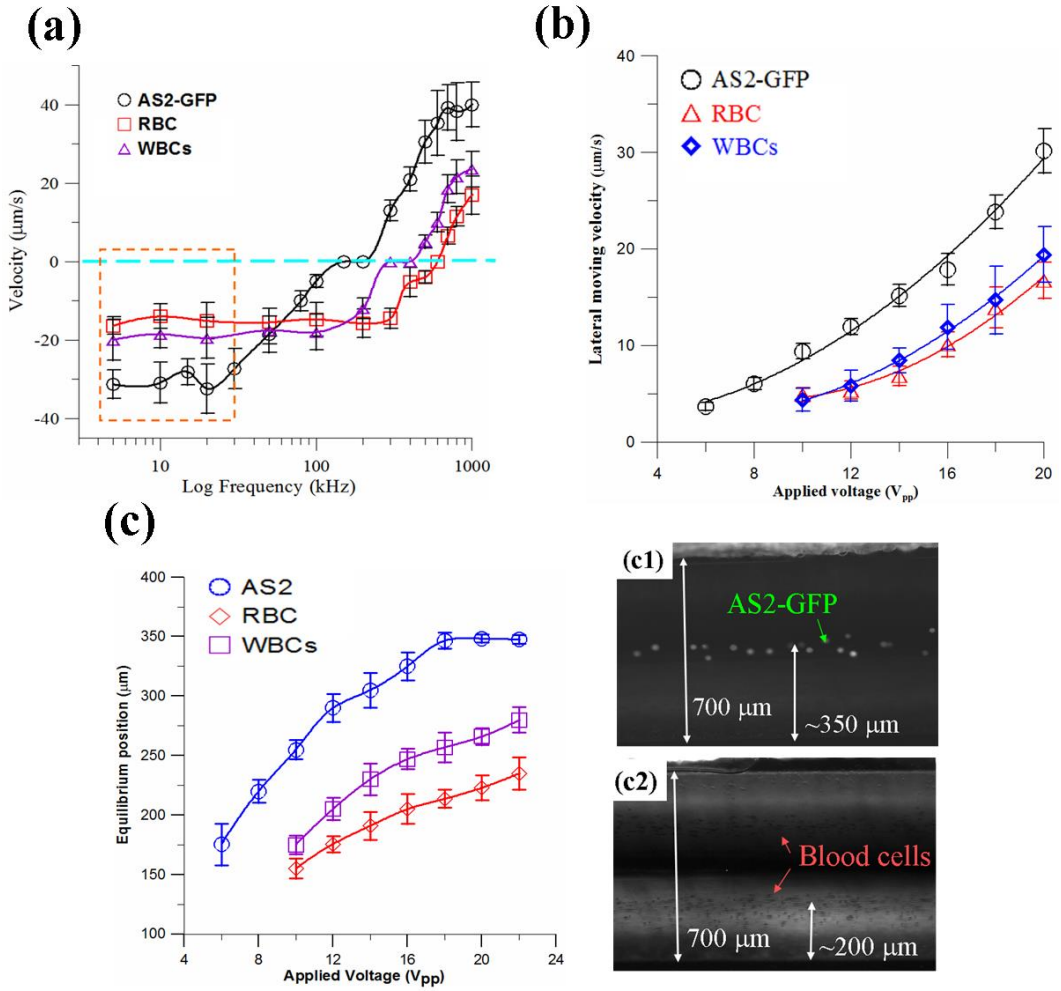

Figure 4

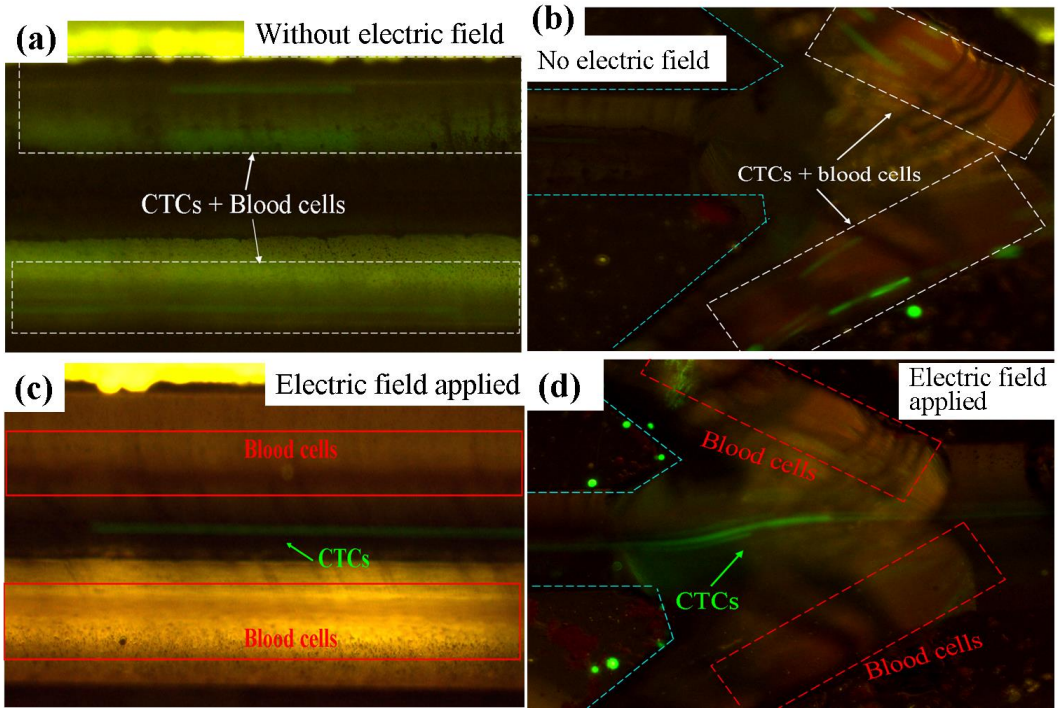

Figure 5

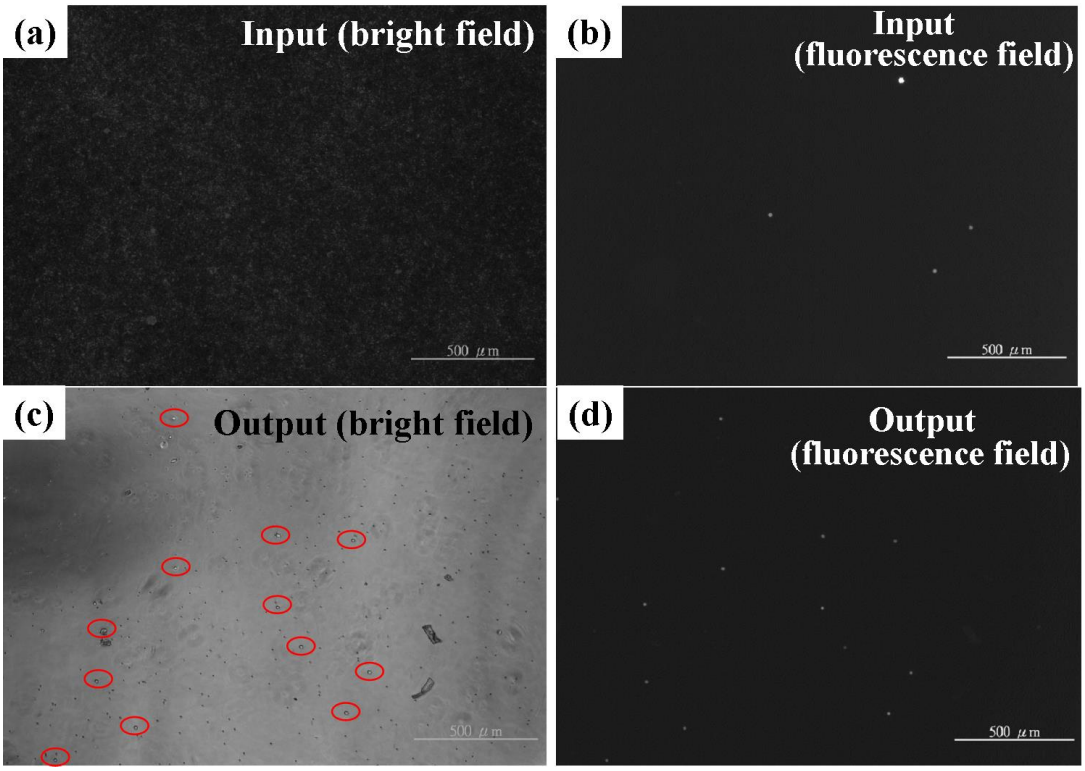

Figure 6